LANGMUIR

pubs.acs.org/Langmuir Article

Biomolecular Surface Functionalization and Stabilization Method to Fabricate Quantum Dots Nanobeads for Accurate Biosensing Detection

Jinjie Li,* Jinjin Fan, Ruili Wu,* Ning Li, Yanbing Lv, Huaibin Shen, and Lin Song Li*

Cite This: *Langmuir* 2022, 38, 4969–4978 Read Online

ACCESS | Metrics & More | Article Recommendations | Supporting Information

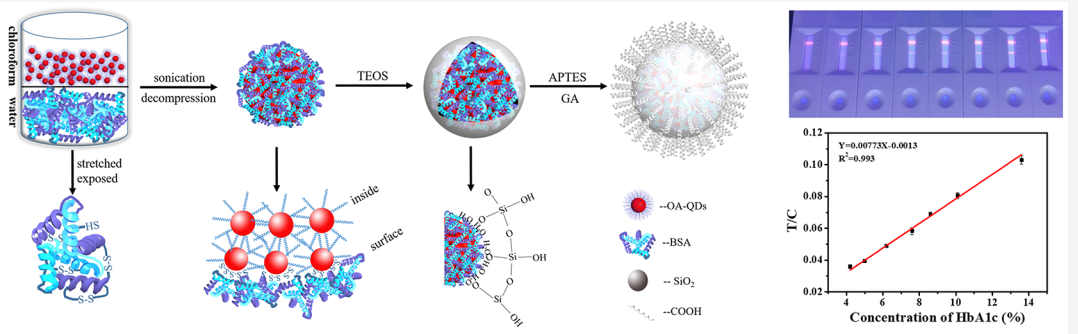

ABSTRACT: The surface functionalization of quantum dots (QDs) is essential for their application as a label material in a biological field. Here, a protein surface functionalization approach was introduced to combine with silica encapsulation for the sustainable and stable synthesis of QDs nanobeads for biomarker detection. The formation of QDs nanobeads was achieved by multiple mercapto groups in bovine serum albumin (BSA) macromolecules as multidentate ligands to replace hydrophobic ligands on the surface of QDs and decompression. The resulting QDs nanobeads exhibited 20 times more photoluminescence than the corresponding hydrophobic QDs and presented excellent stability under physiological conditions due to the protection of BSA and silica. The nanobeads served as a robust signal-generating reagent to construct the lateral flow immunoassay (LFIA) biosensor for the detection of glycosylated hemoglobin (HbA1c). The concentration of HbA1c was determined within 10 min with high specificity using only 60 μL of whole blood samples collected clinically. The nanobeads-based LFIA biosensor exhibited linear detection of HbA1c from 4.2% to 13.6%. The accuracy and stability of this approach in clinical utility was demonstrated by the detection of HbA1c after a long-term storage of test strips. This protein surface modification technology provides a new way for improving the biological properties of QDs in clinical diagnosis.

1. INTRODUCTION

Biologically active surfaces and interfaces generally play an important role in maintaining the properties of materials and hold broad relevance for numerous applications ranging from biomedicine imaging to diagnostics and therapy.[1−3] Therefore, it is necessary to design an effective surface structure that not only can endow materials with good biocompatibility but also can prevent the influence of various complex matrices in the biological environment and improve the stability. Proteins are the basis of life, equipped with various activities and functions, and they have proven to be powerful and versatile molecules. In recent years, growing attention has been focused on functionalizing nanomaterials with some specified proteins due to their simplicity and convenience as well as versatility.[4−6] Great works were devoted to the direct synthesis of nanoparticles in an aqueous solution by using protein, such as bovine serum albumin (BSA), hemoglobin, transferrin, and lysozyme.[7−9] Among them, BSA is the most common functional agent for this purpose, and it can reduce the influence of adverse environmental factors and prevent nonspecific binding of various molecules.[10,11] For example, BSA was coated on the surfaces of gold nanoparticles to block the nonspecific adsorption for chemiluminescence,[12] and the BSA-directed synthesis of MnO_2 was developed to realize the detection of blood glucose.[13] Therefore, BSA has been used as an excellent biologically active surface reagent to endow materials with better properties.

Quantum dots (QDs), as an excellent signal label for producing and transducing the signal, have received increased

Received: February 16, 2022
Revised: March 26, 2022
Published: April 12, 2022

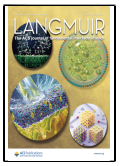

https://doi.org/10.1021/acs.langmuir.2c00392
Langmuir 2022, 38, 4969−4978

attention for biological diagnosis applications.[14−16] The QDs-based lateral-flow immunoassay (LFIA) can improve the sensitivity and convenience on the basis of guaranteeing its original speed and cost-effectiveness, which have become a powerful biosensor for detecting a variety of biomolecules for disease diagnosis.[17−19] Superior bright fluorescence and the high chemical stability of QDs are essential for the sensitivity and accuracy of LFIA. Silica coating can not only ensure the fluorescence performance of QDs but also block the influence of the external environment to a certain extent.[20−22] However, the amorphous nature and mesoporous structure of silica still cannot prevent the interaction between small molecules and QDs even with a thicker silica shell, especially for the detection of whole-blood samples.[23] Taking inspiration from protein modification strategies, attaching biological groups to QDs may make up this shortcoming to improve the stability of QDs in complex matrix. Zhang et al. developed BSA-modified QDs by a phase-transfer method for cell-targeted imaging, and the water solubility and stability of QDs had been significantly improved.[24] But it is inevitable that ligand exchange resulted in the significant reduction of fluorescence performance for hydrophobic QDs. The encapsulation of multiple-QDs into the beads could be brighter than single QDs due to their greater number,[25] which weakened the influence of ligand substitution and further amplified the detectable signal of the biomarkers. Previously, our group prepared nanobeads with strong luminescence and robustness by a chemical bond embedding method and dual protecting strategy, which have been used to build detection platforms with amplified signals and high accuracy in clinical diagnostics.[26,27] It is worthwhile to develop QDs nanobeads by BSA for the quantitative and accurate LFIA-biosensor detection of biomarkers.

In the current study, we first put forward the fabrication of a novel kind of QD nanobead with extraordinary stability by the surface modification using the bio-macromolecule BSA and SiO_2 to develop a more accurate and robust LFIA biosensor for biomarker detection. BSA contains one cysteine and multiple disulfide bonds, which preferentially replace the original hydrophobic ligands on the surface of QDs and further wrap the multiple QDs to form nanobeads under ultrasonication and decompression conditions. The polydentate ligand of BSA is not prone to a photoinduced dimerization of sulfhydryl groups on the particle surface, and the abundant water-soluble groups increase the buffer capacity to the external environment and the ability for growing thicker silica shells. Combined with the silica coating, the obtained QDs@BSA@SiO_2−COOH nanobeads exhibited ∼20 times brighter luminescence than the corresponding hydrophobic QDs and displayed admirable robustness against harsh conditions, such as acid etching, alkali etching, and high temperature. The nanobeads were proposed as a signal amplification probe of an LFIA biosensor for an accurate detection of biomarkers. Glycated hemoglobin (HbA1c) has been regarded as the gold standard[28−30] for long-term glycemic control in diabetes mellitus, which was used as the target analyte to evaluate the performance of QDs@BSA@SiO_2−COOH-based LFIA biosensor. The introduction of BSA macromolecules effectively improved the specific reaction efficiency. As expected, the excellent quantitative detection ability of the nanobeads-based LFIA was observed in a linear range of HbA1c from 4.2% to 13.6% by detecting whole-blood samples collected clinically. The correlation value of 0.973 was obtained by comparing the results with the high-performance liquid chromatographic (HPLC) method, which verified the practicability and effectiveness of QDs@BSA@SiO_2−COOH-based LFIA biosensor. Besides, the admirable stability of the QDs nanobeads coated with thick silica shells and BSA also endowed high accuracy for the detection of glycosylated hemoglobin after long-term storage (Coefficient of variation (CV) < 8%), which showed this new LFIA biosensor held promise as a potential alternative method to analyze HbA1c clinically.

2. EXPERIMENTAL SECTION

2.1. Materials and Apparatus. The details for materials and apparatus were shown in the Supporting Information.

2.2. Synthesis of QDs@BSA. The hydrophobic oleic acid surfactant-capped CdSe/ZnS QDs (PL 620 nm) were synthesized by procedures given in our previous reports,[31,32] and then they were purified and redispersed in chloroform (3.3×10^{-6} M). The weighed BSA was dissolved in 15 mL of ultrapure water. Then, the appropriate amount of QD chloroform solution was added into the BSA solution under the ultrasonication condition (The content of them was adjusted according to the molar ratio of BSA and QDs in the range of 200−2000). The clear, light cyan color solution began to turn cloudy. The emulsion-like solution reacted continuously for 20 min, and then the organic solvent was quickly and completely removed under vacuum decompression to form BSA-encapsulated quantum dot nanobeads (QDs@BSA). The reaction system was centrifuged at 20 000 rpm for 15 min, and the resulting QDs@BSA nanobeads were washed with deionized water to remove unreacted reagents and redispersed in deionized water.

2.3. Synthesis of QDs@BSA@SiO_2−COOH. QDs@BSA@SiO_2−COOH nanobeads were prepared according to the previously reported procedures.[33,34] The mixture of QDs@BSA nanobeads solution, 20 mL of ethanol, and the appropriate amounts of ammonia and tetraethyl orthosilicate (TEOS) was stirred for 24 h at room temperature to form the silica shell. Then, 300 μL of (3-aminopropyl)triethoxysilane (APTES) was added the reaction system to produce the silica surface functionalized with $-NH_2$ groups. For modifying the carboxyl groups on the surface of nanobeads, the obtained amino-functionalized QDs@BSA@SiO_2 was dispersed in dimethyl sulfoxide (DMSO) and reacted with 0.05 g of glutaric anhydride (GA) for 12 h. the resulting QDs@BSA@SiO_2−COOH was centrifuged and dialyzed in deionized water for 24 h. The QDs@BSA@SiO_2−COOH was collected by centrifugation and washed with ethanol three times.

2.4. Preparation of QDs@BSA@SiO_2−COOH-Antibodies Probes. To prepare the QDs@BSA@SiO_2−COOH-antibodies probes, 1-ethyl-3-(3-(dimethylamino) propyl) carbodiimide (EDC) and *N*-hydroxysulfosuccinimide (sulfo-NHS) activation technology was used to activate the carboxyl group of nanobeads, and the antibodies were conjugated to the surface of the nanobeads via a covalent attachment. Generally, 75 μL of QDs@BSA@SiO_2−COOH (2.23×10^{-6} M) was dispersed in sodium borate buffer (BS, 5 mM, pH 7.2) and followed by the addition of 50 μL of 0.045 M EDC and 50 μL of 0.113 M sulfo-NHS. After ultrasonic activation at low temperature for 5 min, the mixed solution was collected by centrifugation and resuspended with 400 μL of BS buffer (5 mM, pH 8.0). Subsequently, 52.5 μg of sheep anti-human hemoglobin polyclonal antibody (Hb) was slowly injected into the above solution and incubated at 4 °C overnight. Then, 1% BSA solution and 2.4 μL of ethanolamine were reacted with the QDs@BSA@SiO_2−COOH-Hb to reduce nonspecific adsorption. Afterward, the obtained QDs@BSA@SiO_2−COOH-Hb probes were centrifuged and washed quintic with BS (5 mM, pH 9.0). Finally, the QDs@BSA@SiO_2−COOH@Hb (T probe) was resuspended in BS buffer solution (5 mM, pH 7.4, 0.5% BSA) and stored at 4 °C for the following tests. The above procedure was also used to prepare QDs@BSA@SiO_2−COOH@rabbit anti-deoxyribo-nucleoprotein antibody (DNP) (C probe).

2.5. Preparation of QDs@BSA@SiO_2−COOH-Based LFIA. Typically, the QDs@BSA@SiO_2−COOH-based LFIA consisted of sample pad, conjugate pad, nitrocellulose (NC) membrane, and

https://doi.org/10.1021/acs.langmuir.2c00392
Langmuir 2022, 38, 4969−4978

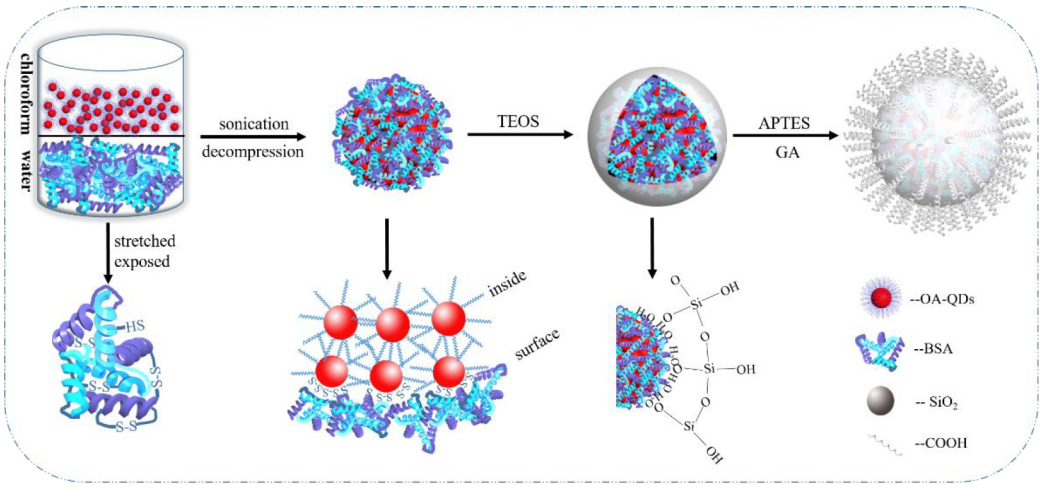

Figure 1. Schematic illustrating the preparation of QDs@BSA@SiO_2−COOH (above) and diagram of the surface-modified structure (below).

absorbent pad loaded on backing card from bottom to top. In order to reduce nonspecific adsorption and increase the signal-to-noise ratio, the sample pads were saturated with BS buffer (2 mM pH 8.0, containing 0.25% casein (w/v) and 0.5% Tween-20 (w/v)). The QDs@BSA@SiO_2−COOH@Hb (T probe) and QDs@BSA@SiO_2−COOH@rabbit anti-deoxyribo-nucleoprotein antibody (C probe) were sprayed on the conjugation pad with an appropriate spraying amount and dried at 37 °C in a vacuum drying oven. The test zone and control zone were obtained, respectively, with the desired volume of mouse anti-human HbA1c antibody (capture antibody, 1 mg mL^{-1}) and anti-deoxyribo-nucleoprotein antibody-BSA (DNP-BSA, 0.5 mg mL^{-1}) diluted in phosphate buffer (PBS, 10 mM, pH 7.4) on the nitrocellulose membrane. After 16 h of incubation at 37 °C, all of the parts mentioned above were attached on the back plates overlapping 2 mm on top of each other successively. Finally, the assembly was cut into 4 mm wide strips and stored at room temperature in the dry environment before use.

2.6. Clinical Sample. The clinical samples of HbA1c ranged from 4.2% to 13.6% were collected by using commercial collection tubes containing anticoagulant (containing 3.7−5.4 μmol/mL of ethylenediaminetetraacetic acid (EDTA)) and heparin sodium (12−30 IU/mL). 34 clinical whole-blood samples from Taizhou People's Hospital were approved by the Biomedical Research Ethics Committee of Henan University (HUSOM-2022-139). The sample should be shook well and stored at 2−8 °C until further use. The concentrations of HbA1c were determined and compared by using QDs@BSA@SiO_2−COOH-based LFIA and commercial HPLC.

3. RESULTS AND DISCUSSION

3.1. Formation Mechanism of QDs@BSA Nanobeads. Fabrication of the QDs@BSA@SiO_2−COOH was illustrated in Figure 1. The surface functionalization of QDs by BSA was the key factor to the formation of nanobeads. The assumption of the formation process of QDs@BSA nanobeads was put forward as follows: Under the ultrasonic condition, the chloroform solution containing QDs was dispersed in an aqueous solution of BSA to form microemulsion droplets and achieve a dynamically stable state. The amount of BSA was not enough for effective ligand exchange between BSA and the pendant fatty acid chains on the surface of QDs. One single cysteine and eight pairs of disulfide bonds of BSA were stretched and exposed, which preferentially replaced the original organic ligands on the surface of QDs outside the droplet. The chloroform of the droplet was rapidly volatilized under reduced pressure, and thus the multiple QDs with the original ligand were wrapped in BSA to form nanobeads. This hypothesis was verified by the following experimental results. The TEM results of different mole ratios of BSA to QDs were shown in Figure S1 (Supporting Information). When the molar ratio of BSA to QDs was 2000:1, the QDs were monodisperse without aggregation under the electron microscope field, indicating that the content of BSA was sufficient to modify all QDs. The prepared samples gradually aggregated into beads with the proportion of QDs increased. The explanation for this aggregation was that the hydrophobic surfactants of QDs were not efficiently replaced by the limited BSA macromolecules at low mole ratios of BSA/QD, and BSA preferentially reacted with QDs on the outer layer of hydrophobic droplets. With excess QDs addition, the degree of aggregation of QDs was uncontrollable and showed no longer water solubility. The TEM analysis further confirmed that the less of BSA, the larger size and the more regular shape of the nanobeads in a certain range. Ultrasonication was also a prerequisite for the preparation of nanobeads, which was used to promote the formation of an oil-in-water system and expose the sulfhydryl and disulfide bonds of BSA to replace the oleic acid ligand on the surface of QDs. Although magnetic stirring could make the system bearing emulsion-like property by dispersing QDs in the aqueous solution of BSA, the obtained sample was not biocompatible, indicating that the importance of ultrasound for BSA-modified QDs. Moreover, the changes of ultrasonic power also affected the formation of nanobeads. When the ultrasonic power was insufficient, the chloroform solution containing QDs could not be completely dispersed in the aqueous solution of BSA and presented a stratification phenomenon. At the same time, the dynamic equilibrium of microemulsion droplets was destroyed with the excessive increase of ultrasonic power, resulting in partly modified single QDs. As a result, the microemulsion droplets were formed and achieved a dynamically stable state at 300−500 W ultrasound power. The effect of decompression conditions on the morphology of nanobeads was also monitored by TEM (Figure S2, Supporting Information). Under the condition of reduced pressure, the chloroform was volatilized rapidly, and QDs without ligand exchange inside the droplet were confined to form nanobeads (Figure S2a, Supporting Information). On the contrary, QDs showed disorder without decompression (Figure S2b, Supporting Information), indicating the necessity of decompression conditions. The decompression condition only needed to meet the requirement of accelerating

https://doi.org/10.1021/acs.langmuir.2c00392
Langmuir 2022, 38, 4969−4978

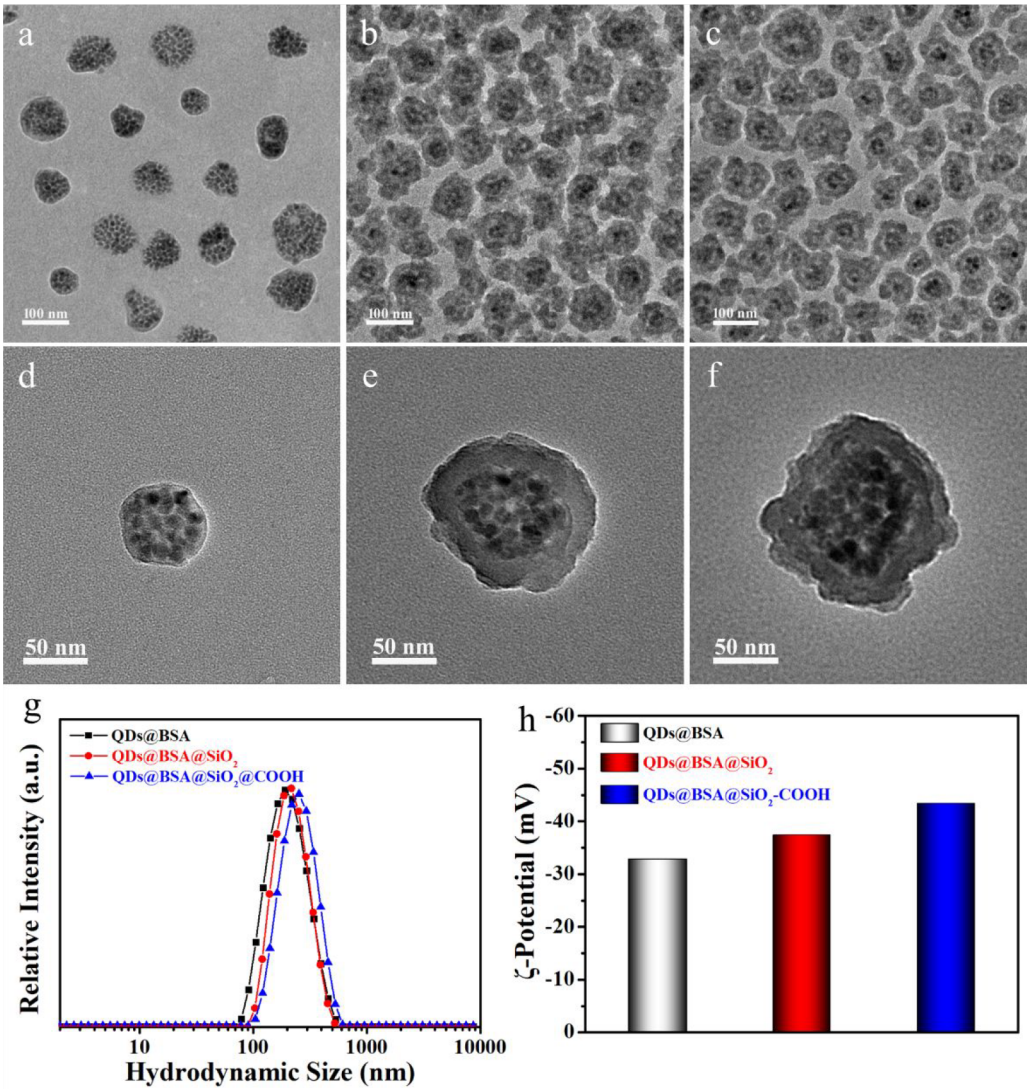

Figure 2. TEM images of (a) QDs@BSA, (b) QDs@BSA@SiO_2, (c) QDs@BSA@SiO_2−COOH, (d) a single QDs@BSA, (e) a single QDs@BSA@SiO_2, and (f) a single QDs@BSA@ SiO_2−COOH. (g) The DLS data and (h) zeta potential changes in the preparation of QDs@BSA@ SiO_2−COOH nanobeads.

chloroform volatilization. The zeta potential of QDs@BSA and BSA approached 0 at pH 5 attributable to the isoelectric point of BSA in this pH range, and the values were almost consistent at pH 7 and 9 (Figure S3, Supporting Information), indicating that carboxyl and amino groups of BSA did not involve in the surface modification of the QDs and endowed the nanobeads with water solubility. The above conclusions verified the assumption about the formation mechanism of QDs@BSA nanobeads.

3.2. Characterization of QDs@BSA@SiO_2−COOH Nanobeads. The synthesized CdSe/ZnS QDs through the phosphine-free method showed good monodispersion and uniformity in size with an average diameter of 14 ± 1.5 nm (Figure S4, Supporting Information). Modified with BSA, the nanobeads with near-spherical shape were formed and well-dispersed on the copper mesh, which was shown in Figure 2a. Owing to the randomness of the droplet shape formed by chloroform dispersing in the BSA aqueous solution, the morphology of nanobeads was irregular, and the size also had a certain distribution (78 ± 20 nm). The higher-magnification TEM image demonstrated that each nanobead was composed of loose-packed multiple QDs (the distance of QDs was ∼2.5 nm) and the outer layer had obvious BSA boundaries (Figure 2d). Combined with the particle sizes of QDs themselves (14 ± 1.5 nm), the center-to-center distance between QDs in the QDs@BSA was significantly greater than the distance of energy resonance transmission (7−10 nm). As a bioactive group, BSA could also protect the QDs in the nanobeads from the influence of the external environment to a certain extent, and thereby it make up for the defects of the porous structure of silica. The nanobeads were further coated by silica shell to enhance the stability. The amino and carboxyl groups of BSA could endow the nanobeads with water solubility, which was helpful to prepare the thick silica shell. As shown in Figure 2b, by the encapsulation of SiO_2 layers on the nanobeads, QDs@BSA@SiO_2 were successfully obtained with an average diameter of 112 ± 25 nm. Obviously, silica layers showed lower contrast in the TEM image and completely surrounded the surface of the nanobeads. The nanobeads displayed nanoscale roughness and no obvious aggregation. The TEM characterization of single QDs@BSA@SiO_2 nanobeads in Figure 2e showed that silica was coated on the surface of the

https://doi.org/10.1021/acs.langmuir.2c00392
Langmuir 2022, 38, 4969−4978

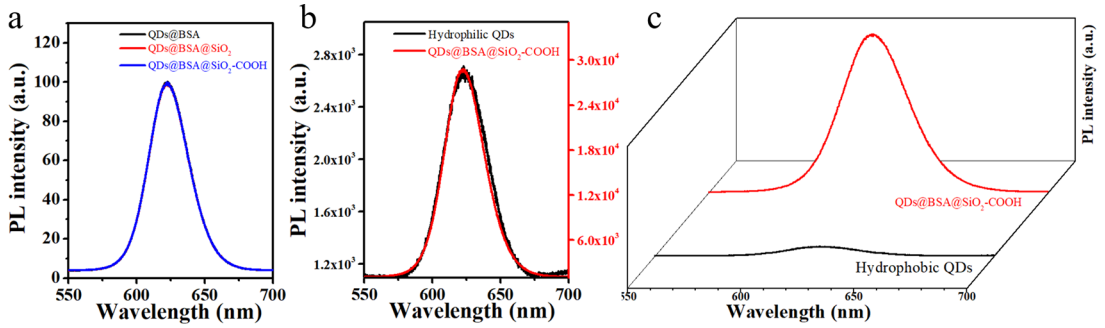

Figure 3. (a) Comparison of PL emission peaks in the preparation of QDs@BSA@SiO_2−COOH nanobeads. (b) identical fluorescence emission spectra of QDs@BSA@SiO_2−COOH and hydrophobic QDs. (c) fluorescence spectra of QDs@BSA@SiO_2−COOH and hydrophobic QDs at the same particle concentration.

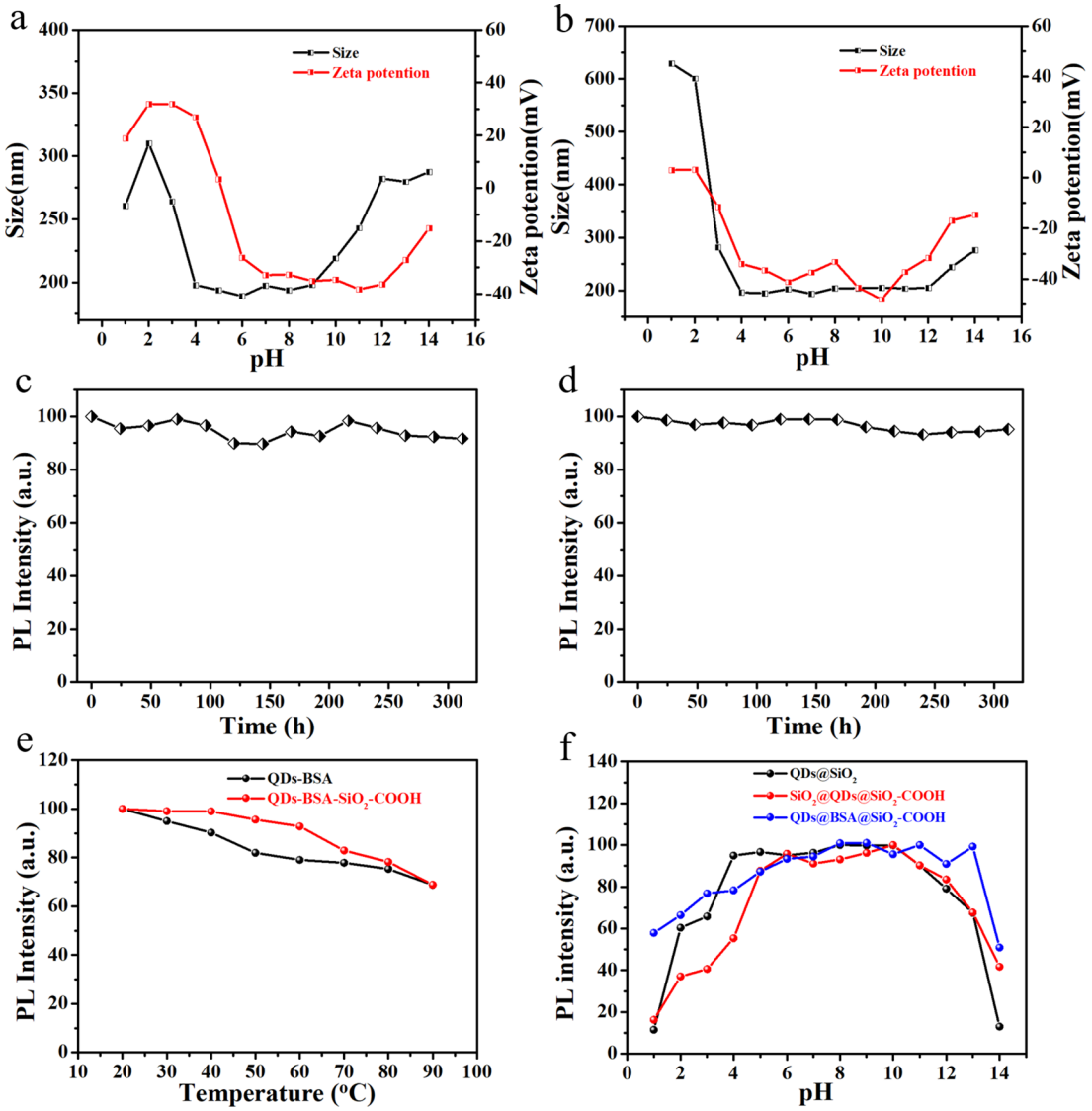

Figure 4. Hydrodynamic size and zeta potential of (a) QDs@BSA and (b) QDs@BSA@SiO_2−COOH nanobeads in different pH values. effects of (c) ultraviolet lighting, and (d) storage times at 60 °C on the photoluminescence of QDs@BSA@SiO_2−COOH. (e) thermal stability comparison of QDs@BSA and QDs@BSA@SiO_2−COOH. (f) pH stability comparison of QDs@SiO_2, SiO_2@QDs@SiO_2−COOH, and QDs@BSA@SiO_2−COOH.

nanobeads layer by layer, corresponding to the gradual hydrolysis process of TEOS, indicating that the water solubility of BSA effectively improved the hydrolysis ability of TEOS. The thickness of the silica shell fluctuated in the range of 25−30 nm according to the hydrolysis degree of TEOS, which was caused by the irregular shape of nanobeads. It can be seen from Figure 2c,f that the structure of the nanobeads with carboxyl group modification was almost identical with those coated by

https://doi.org/10.1021/acs.langmuir.2c00392
Langmuir 2022, 38, 4969−4978

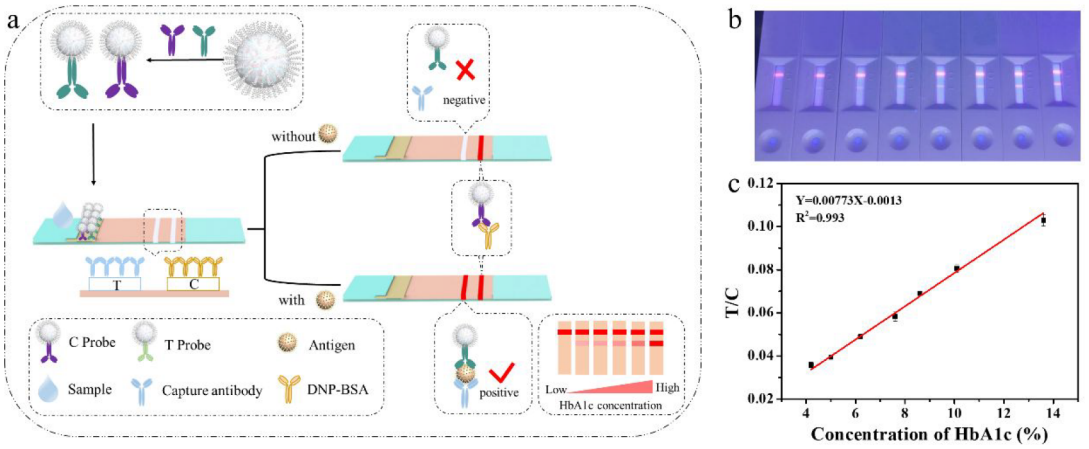

Figure 5. (a) Schematic illustration of QBs@SiO_2−COOH-based LFIA biosensor for HbA1 detection. (b) Fluorescence pictures of standard HbA1c standard solution detected by QDs@BSA@SiO_2−COOH-based LFIA. (c) QDs@BSA@SiO_2−COOH-based LFIA linear response for HbA1c quantitative detection.

silica. To further confirm the successful synthesis of QDs@BSA@SiO_2−COOH, dynamic light scattering (DLS) was employed to monitor the hydrodynamic diameters and zeta potentials during the process of synthesis. As shown in Figure 2g, the hydrodynamic size of QDs@BSA was larger than the real particle size observed from TEM due to the swollen corona of BSA macromolecules dispersing in the aqueous solution. After silica coating, the hydrodynamic size of nanobeads increased from 192.3 to 206.6 nm. The magnitude of the increase was not completely consistent with the thickness of silica shell in TEM image, indicating that the coating of silica made the BSA macromolecules more compact. The hydrodynamic size of QDs@BSA@SiO_2−COOH further increased to 216 nm, which proved the successful functionalization of hydrophilic layers. The zeta potential changes of QDs@BSA, QDs@BSA@SiO_2, and QDs@BSA@SiO_2−COOH indicated the gradual increase in stability and also confirmed the synthesis process of nanobeads (Figure 2h).

The comparison of PL emission peaks in the preparation of QDs@BSA@SiO_2−COOH nanobeads was shown in Figure 3a. The spectra were normalized to the emission maximum of each sample. The identical fluorescence emission spectra indicated that there was almost no QDs loss during the silicon coating and carboxylation process, which proved the reproducibility of the experimental scheme. Moreover, Figure 3b was to verify the changes of emission peak and full width at half-maximum of nanobeads and hydrophobic QDs, and the result was not easy to be observed because the nanobeads had stronger photoluminescence than that of QDs. As a result, two ordinates were established to make the emission peaks in the same region. The result showed the nanobeads modified by BSA had the same emission peak as hydrophobic QDs, indicating that the construction of QDs@BSA@SiO_2−COOH did not affect the properties of QDs. Theoretically, ligand exchange can usually cause the decrease of fluorescence intensity due to the change of the original ligand of QDs. During the formation of nanobeads, BSA preferentially replaced the original hydrophobic ligands on the surface of QD outside the droplet during the formation of nanobeads, and the QDs inside still maintained the original luminous efficiency. So the nanobead containing multiple QDs was considered as a single particle to be compared with the fluorescence properties of hydrophobic QDs at the same particle concentration. It can be seen from Figure 3c that QDs@BSA@SiO_2−COOH nanobeads exhibited much stronger fluorescence intensity (~20 times) than the hydrophobic QDs. The above results showed that the water-soluble QDs@BSA@SiO_2−COOH nanobeads with high fluorescence were successfully prepared by using the biological macromolecule BSA.

3.3. Colloidal Stability of QDs@BSA@SiO_2−COOH Nanobeads. Colloidal stability is a key factor to guarantee the ability of BSA-modified nanobeads to be used in *in vitro* diagnosis. Figure 4a,b showed the hydrodynamic diameters and zeta potentials of QDs@BSA and QDs@BSA@SiO_2−COOH at various pH values. It is well-known that BSA has an effective buffering capacity in acidic and alkaline solutions due to its amino and carboxyl groups. Therefore, the particle size of the BSA-modified nanobeads remained basically unchanged in the range of pH 4−9. The zeta potentials of QDs@BSA showed that the large quantity of amino and carboxyl groups on BSA macromolecules rendered QDs@BSA with strong stability (>30 mV or ≤30 mV) in the range of pH <5 and pH >6. The electrical neutrality was observed at pH 5, attributable to the isoelectric point of BSA in this pH value. The phenomenon disappeared after modification with the silica shell and carboxyl group, and QDs@BSA@SiO_2−COOH nanobeads preserved high stability over the wide pH range of 4−12. In order to further verify the stability of QDs@BSA@SiO_2−COOH, the fluorescence stability of QDs@BSA@SiO_2−COOH at various biological environments was carefully monitored. The result of photostability was shown in Figure 4c, and the fluorescence of QDs@BSA@SiO_2−COOH still maintained more than 90% by illuminating with a 365 nm ultraviolet lamp in 300 h. When the QDs@BSA@SiO_2−COOH were stored at 60 °C for 300 h, a little change in the photoluminescence intensity was observed (<5%), indicating that long-term storage had almost no effect on the fluorescence performance of QDs@BSA@SiO_2−COOH (Figure 4d). The results of the PL intensity of nanobeads in different temperatures were shown in Figure 4e, and it can be seen that the dual protection of silica shell and BSA endowed the QDs@BSA@SiO_2−COOH nanobeads stronger thermal stability. Figure 4f exhibited the fluorescence properties of QDs@BSA@SiO_2−COOH, QDs@SiO_2, and SiO_2@QDs@SiO_2−COOH nanobeads (prepared according to procedures given

https://doi.org/10.1021/acs.langmuir.2c00392
Langmuir 2022, 38, 4969−4978

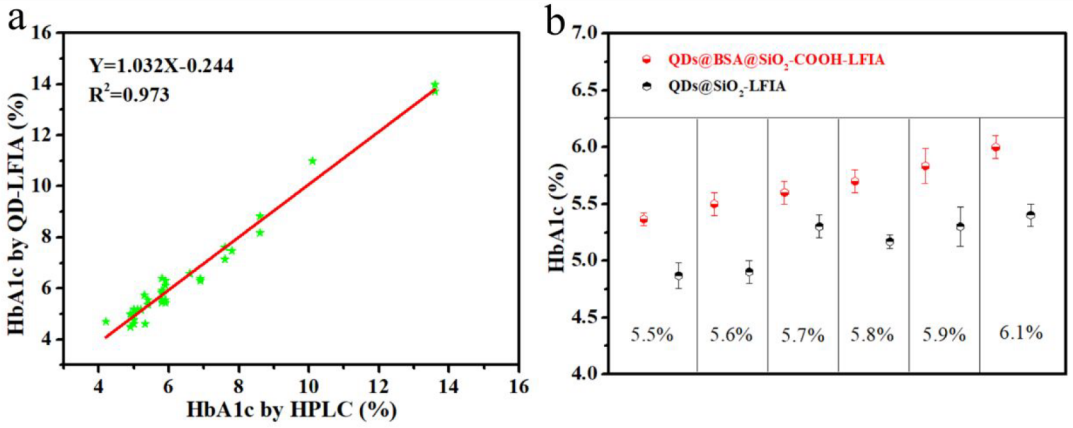

Figure 6. (a) Comparison for clinical HbA1c samples detected by QDs@BSA@SiO_2−COOH-based LFIA and HPLC (N = 34). (b) Results of the clinical samples analyzed with the QDs@BSA@SiO_2−COOH-based LFIA (red dots) and QDs@SiO_2-based LFIA (black dots) stored at room temperature after 70 d.

in ref 35) after being preserved for 1 h at various pH conditions. The silica shell could block the influence of the external environment to a certain extent. In some case, the amorphous nature of the silica shell and their mesopores provided channel for small molecules to damage the properties of QDs. The QDs@BSA@SiO_2−COOH nanobeads were much less vulnerable to strong acids and alkali conditions than others. Such great improvement of the pH stability was attributable to the distinctive buffer capability of BSA, which demonstrated that the introduction of BSA had a positive effect on the stability of the QDs@BSA@SiO_2−COOH nanobeads. The above results showed that the combination of BSA and SiO_2 protection endowed QDs@BSA@SiO_2−COOH nanobeads with strong stability.

3.4. Fabrication of QDs@BSA@SiO_2−COOH-Based LFIA for HbA1c Detection. The principle assay of QDs@BSA@SiO_2−COOH-based LFIA for a quantitative detection of HbA1c was depicted in Figure 5a. The detection of HbA1c by the LFIA was performed based on the formation of the T probe/HbA1c/antibody sandwich structure. The whole-blood sample after dilution was added to the sample pad, and the capillary force generated by the high hydrophilicity and porous structure of NC membrane will make it flow along the test strip. Generally, if the HbA1c antigen was contained in the sample, it combined with T probe on the conjugated pad and then was captured by the coating antibody (HbA1c antibody) on the test line via an antigen−antibody reaction to generate a positive signal. The control line was formed by the migration of the C probe along the NC membrane and combination specifically with the coating antibody (DNP-BSA). If there was no HbA1c antigen in the sample, the negative result was determined because only the signal of the control line can be detected. The signal values of T and C lines could be obtained by the NepQD-Infinity-V1 (excited by 365 UV light-emitting diode (LED) light) because of the high fluorescence intensity and signal-to-noise ratio of nanobeads. The signal value of the T line increased with the increase of HbA1c concentration. Consequently, the qualitative detection of HbA1c in the sample could be achieved by calculating the fluorescence intensity ratio between the test line and the control line (T/C).

3.5. Analytical Performance of QDs@BSA@SiO_2−COOH-Based LFIA. To achieve the best detection performance, the mole ratio of nanobeads to antibodies was optimized and shown in Figure S5a (Supporting Information). Because the insufficient amount of antibody on the surface of nanobeads (the coupling ratio was 1:1) cannot fully bind to the antigen in the sample, the T/C value was relatively low. With the increase of antibody coupling ratio, the detection results showed the higher T/C value under different HbA1c concentration conditions. When the antibody coupling ratio was 1:2, the fold ratio of T/C was consistent with the fold ratio of HbA1c concentration, which had a better linear relationship. Thus, 1:2 was selected as the optimal mole ratio. Furthermore, a certain amount of probes was sprayed on the conjugated pad in the test strip and combined with the antigen in the simple to realize quantitative detection. As shown in Figure S5b (Supporting Information), insufficient T probes (0.03 μL cm^{-1}) resulted in lower T/C values, and 0.08 μL cm^{-1} of sufficient probes showed the highest T/C values. However, too much addition of the spraying amount caused the weakening release ability and flow capacity of the fluorescence probes. It can be seen that a few T probes were remained on the conjugate pad and NC membrane when the T probe spraying amount was 0.08 μL cm^{-1}, which could result in a higher background noise (Figure S5b inset, Supporting Information). As a result, the optimum spraying amount of the T probe was 0.06 μL cm^{-1}. The effective reaction time, ranging from 6 to 15 min, was determined by using the whole-blood samples containing different concentrations of HbA1c. As displayed in Figure S5c (Supporting Information), the T/C value increased gradually with the extension of detection time, which reached the highest value in 10 min and remained basically constant. Thus, the quantitative detection time of HbA1c was chosen as 10 min.

After optimizing the detection conditions, the analytical performance of LFIA based on QDs@BSA@SiO_2−COOH was evaluated by the quantitative detection of HbA1c antigen. HbA1c whole-blood samples with different concentrations (4.2%, 5.0%, 6.2%, 7.6%, 8.6%, 10.1%, 13.6%) were diluted 100 times with sample dilution (2 mM boric acid, pH 6.3, 1% Tritonx-100, 1% tween 20), and the T/C values were obtained after 10 min of immune reaction time by loading 60 μL of the diluted whole-blood sample onto the sample pad of LFIA. Figure 5b revealed that the higher the concentration of glycosylated hemoglobin, the stronger the signal value of the T

https://doi.org/10.1021/acs.langmuir.2c00392
Langmuir 2022, 38, 4969−4978

zone. The corresponding T/C ratios also increased obviously. There was no probe remained on the surface of the test strip, indicating that the whole-blood sample did not cause the increase of background signal. As indicated in Figure 5c, the calibration curve exhibited an excellent linear range from 4.2% to 13.6% with a reliable correlation coefficient (R^2 = 0.993). The regression equation could be represented by Y = 0.007 73X − 0.0013, where Y was the T/C, and X was the HbA1c concentration. Error bars expressed the standard deviation of the mean over the three duplicate measurements at different HbA1c concentrations. Such an excellent linear relationship showed that the dual protecting strategy of BSA and silica effectively blocked the influence of the complex matrix in whole-blood samples and effectively ensured the accurate and quantitative detection of HbA1c in whole-blood samples. The intra- and interassays were conducted to evaluate the accuracy and precision of QDs@BSA@SiO_2−COOH-LFIA by analyzing 6.0% and 7.2% HbA1c whole-blood samples. As the results show in Table S1 (Supporting Information), the intra-assay CV and interassay CV of the two samples detected by QDs@BSA@SiO_2−COOH-LFIA was 4.22−7.21% and 5.15−5.95% respectively, which confirmed the high reproducibility and good precision of the assay for the HbA1c analysis. Moreover, compared with the other methods for HbA1c detection,[36−38] this work had demonstrated obvious advantages in linear range, detection time, and stability (shown in Table S2, Supporting Information).

3.6. Robustness of QDs@BSA@SiO_2−COOH-Based LFIA for Clinical Application. To evaluate the potential clinical application of the QDs@BSA@SiO_2−COOH-based LFIA, the results from the new LFIA platform were compared with the HPLC method by analyzing 34 HbA1c whole-blood samples. As shown in Figure 6a, two methods exhibited good agreement with a highly significant correlation of R^2 = 0.973 (>0.95). And the proposed LFIA could complete the sample analysis in 10 min, which was more convenient and effective. HbA1c has been used as a diagnostic indicator for diabetes, which is more reproducible, provides a better reflection of chronic glucose exposure, and correlates well with diabetes-related complications. Several studies showed that the optimal HbA1c cutoff for diagnosing diabetes was between 5.6% and 6.0% in Asian patients, and 6% was set as the optimal HbA1c cutoff values for diabetes and prediabetes by doctors in a clinical diagnosis.[39,40] For a clinical application, it is very important that the QDs@BSA@SiO_2−COOH-based LFIA can accurately distinguish the negative or positive samples of HbA1 above and below 6%, and so the stability of the detection results was essential to its accuracy. In order to verify that the nanobeads with BSA and silica dual encapsulation strategy had a positive effect on the stability of the LFIA platform, clinical HbA1c samples with around cutoff value (5.5%, 5.6%, 5.7%, 5.8%, 5.9%, and 6.3% respectively) were determined by QDs@BSA@SiO_2−COOH-based LFIA and the QDs@SiO_2-based LFIA strips at room temperature for 70 d storage (Figure 6b). The results of QDs@BSA@SiO_2−COOH-based LFIA were almost unchanged, while QDs@SiO_2-based LFIA showed the decrease in assay results, which indicated that the BSA-protected nanobeads endowed a good repeatability and storage stability for the test strips. Therefore, the above results showed that QDs@BSA@SiO_2−COOH-based LFIA demonstrated promise for the quantitative detection of HbA1c in clinical applications.

4. CONCLUSIONS

In this study, fluorescent nanobeads were successfully prepared by biomacromolecule BSA modification and SiO_2 coating. BSA, as a protective layer, made up for the porous defects of silica and improved the stability of QDs, and the rich amino and carboxyl groups of BSA also maintained the optical properties of QDs even in harsh conditions and promoted the growth of silica shell. The obtained QDs@BSA@SiO_2−COOH nanobeads showed advantages of highly luminescence, strong pH buffer capacity and colloidal stability, which have great potential in fields of clinical diagnosis. The resulting nanobeads were used as an excellent signal probe to develop the LFIA for the accurate and quantitative detection of HbA1c, and the detection range of 4.2%−13.6% was successfully realized for the whole-blood samples. And even after a long time of preservation, the detection results of clinical samples detected by the QDs@BSA@SiO_2−COOH-based LFIA biosensor also demonstrated the acceptable accuracy, precision, and stability due to the dual protection of BSA and SiO_2. Given the above, the biomolecular surface modification method endowed high fluorescence, high stability, and excellent label performance for QDs, which opened up a new approach for the surface functionalization of nanoparticles in biological fields.

■ ASSOCIATED CONTENT

Supporting Information

The Supporting Information is available free of charge at https://pubs.acs.org/doi/10.1021/acs.langmuir.2c00392.

Additional information as noted in the text, including the experimental materials, synthesis of hydrophobic CdSe/ZnS QDs, characterization of the QDs, and nanobeads formation process, optimization of the detection conditions, and the stability and reproducibility of nanobeads-based LFIA used in this work (PDF)

■ AUTHOR INFORMATION

Corresponding Authors

Ruili Wu − *Key Laboratory for Special Functional Materials of the Ministry of Education, Henan University, Kaifeng 475004, P. R. China;* orcid.org/0000-0002-6667-5903; Email: wrl0378@henu.edu.cn

Lin Song Li − *Key Laboratory for Special Functional Materials of the Ministry of Education, Henan University, Kaifeng 475004, P. R. China;* orcid.org/0000-0001-7015-3211; Email: lsli@henu.edu.cn

Jinjie Li − *Key Laboratory for Special Functional Materials of the Ministry of Education, Henan University, Kaifeng 475004, P. R. China; School of Chemistry and Chemical Engineering, Henan University of Technology, Zhengzhou 450001, P. R. China*; Email: lijinjie@haut.edu.cn

Authors

Jinjin Fan − *Key Laboratory for Special Functional Materials of the Ministry of Education, Henan University, Kaifeng 475004, P. R. China*

Ning Li − *Key Laboratory for Special Functional Materials of the Ministry of Education, Henan University, Kaifeng 475004, P. R. China*

Yanbing Lv − *Key Laboratory for Special Functional Materials of the Ministry of Education, Henan University, Kaifeng 475004, P. R. China*

https://doi.org/10.1021/acs.langmuir.2c00392
Langmuir 2022, 38, 4969−4978

Huaibin Shen − *Key Laboratory for Special Functional Materials of the Ministry of Education, Henan University, Kaifeng 475004, P. R. China;* orcid.org/0000-0002-6425-0514

Complete contact information is available at: https://pubs.acs.org/10.1021/acs.langmuir.2c00392

Notes

The authors declare no competing financial interest.

■ ACKNOWLEDGMENTS

The authors gratefully acknowledge the financial support from National Natural Science Foundation of China (Grant Nos. 81902158 and 21671058).

■ REFERENCES

(1) Algar, W. R.; Massey, M.; Rees, K.; Higgins, R.; Krause, K. D.; Darwish, G. H.; Peveler, W. J.; Xiao, Z.; Tsai, H. Y.; Gupta, R.; Lix, K.; Tran, M. V.; Kim, H. Photoluminescent nanoparticles for chemical and biological analysis and imaging. *Chem. Rev.* **2021**, *121*, 9243−9358.

(2) Heuer-Jungemann, A.; Feliu, N.; Bakaimi, I.; Hamaly, M.; Alkilany, A.; Chakraborty, I.; Masood, A.; Casula, M. F.; Kostopoulou, A.; Oh, E.; Susumu, K.; Stewart, M. H.; Medintz, I. L.; Stratakis, E.; Parak, W. J.; Kanaras, A. G. The role of ligands in the chemical synthesis and applications of inorganic nanoparticles. *Chem. Rev.* **2019**, *119*, 4819−4880.

(3) Zhang, L. J.; Xia, L.; Xie, H. Y.; Zhang, Z. L.; Pang, D. W. Quantum dot-based biotracking and biodetection. *Anal. Chem.* **2019**, *91*, 532−547.

(4) Diaz, V.; Ramirez-Maureira, M.; Monras, J. P.; Vargas, J.; Bravo, D.; Osorio-Roman, I. O.; Vasquez, C. C.; Perez-Donoso, J. M. Spectroscopic properties and biocompatibility studies of cdte quantum dots capped with biological thiols. *Sci. Adv. Mater.* **2012**, *4*, 609−616.

(5) Sapsford, K. E.; Algar, W. R.; Berti, L.; Gemmill, K. B.; Casey, B. J.; Oh, E.; Stewart, M. H.; Medintz, I. L. Functionalizing nanoparticles with biological molecules: developing chemistries that facilitate nanotechnology. *Chem. Rev.* **2013**, *113*, 1904−2074.

(6) Aires, A.; Möller, M.; Cortajarena, A. L. Protein design for the synthesis and stabilization of highly fluorescent quantum dots. *Chem. Mater.* **2020**, *32*, 5729−5738.

(7) Wei, H.; House, S.; Wu, J.; Zhang, J.; Wang, Z.; He, Y.; Gao, E. J.; Gao, Y.; Robinson, H.; Li, W.; Zuo, J.; Robertson, I. M.; Lu, Y. Enhanced and tunable fluorescent quantum dots within a single crystal of protein. *Nano Res.* **2013**, *6*, 627−634.

(8) Zhou, W.; Baneyx, F. Biofabrication of ZnS:Mn luminescent nanocrystals using histidine, hexahistidine, and His-tagged proteins: A comparison study. *Biochem. Eng. J.* **2014**, *89*, 28−32.

(9) Lee, J. Y.; Kim, J. S.; Park, J. C.; Nam, Y. S. Protein-quantum dot nanohybrids for bioanalytical applications. Wires. *WIRES Nanomed. Nanobi.* **2016**, *8*, 178−190.

(10) Wakayama, J.; Sekiguchi, H.; Akanuma, S.; Ohtani, T.; Sugiyama, S. Methods for reducing nonspecific interaction in antibody-antigen assay via atomic force microscopy. *Anal. Biochem.* **2008**, *380*, 51−58.

(11) Ledesma, A. E.; Chemes, D. M.; Frias, M. d. l. A.; Guauque Torres, M. d. P. Spectroscopic characterization and docking studies of ZnO nanoparticle modified with BSA. *Appl. Surf. Sci.* **2017**, *412*, 177−188.

(12) Huang, Y.; Gao, L.; Cui, H. Assembly of multifunctionalized gold nanoparticles with chemiluminescent, catalytic, and immune activity for label-free immunoassays. *ACS Appl. Mater. Interfaces.* **2018**, *10*, 17040−17046.

(13) Han, L.; Zhang, H.; Chen, D.; Li, F. Protein-directed metal oxide nanoflakes with tandem enzyme-like characteristics: colorimetric glucose sensing based on onepot enzyme-free cascade catalysis. *Adv. Funct. Mater.* **2018**, *28*, 1800018.

(14) Gao, X.; Cui, Y.; Levenson, R. M.; Chung, L. W. K.; Nie, S. In vivo cancer targeting and imaging with semiconductor quantum dots. *Nat. Biotechnol.* **2004**, *22*, 969−976.

(15) Michalet, X.; Pinaud, F. F.; Bentolila, L. A.; Tsay, J. M.; Doose, S.; Li, J. J.; sundaresan, G.; Wu, A. M.; Gambhir, S. S.; Weiss, S. Quantum dots for live cells, in vivo imaging, and diagnostics. *Science* **2005**, *307*, 538−544.

(16) Zhang, L. J.; Xia, L.; Xie, H. Y.; Zhang, Z. L.; Pang, D. W. Quantum dot based biotracking and biodetection. *Anal. Chem.* **2019**, *91*, 532−547.

(17) Quesada-González, D.; MerkoçI, A. Nanoparticle-based lateral flow biosensors. *Biosens. Bioelectron.* **2015**, *73*, 47−63.

(18) Song, Y.; Sun, J.; Zhao, S.; Gao, F.; Yuan, H.; Sun, B.; Wang, B.; Wang, Y. Based lateral flow immunosensor for ultrasensitive and selective surface-enhanced Raman spectroscopy stroke biomarkers detection. *Appl. Surf. Sci.* **2022**, *571*, 151153.

(19) Wu, R.; Zhou, S.; Chen, T.; Li, J.; Shen, H.; Chai, Y.; Li, L. S. Quantitative and rapid detection of C-reactive protein using quantum dot-based lateral flow test strip. *Anal. Chim. Acta* **2018**, *1008*, 1−7.

(20) Zhou, Z.; Ying, H.; Liu, Y.; Xu, W.; Yang, Y.; Luan, Y.; Lu, Y.; Liu, T.; Yu, S.; Yang, W. Synthesis of surface molecular imprinting polymer on SiO_2-coated CdTe quantum dots as sensor for selective detection of sulfadimidine. *Appl. Surf. Sci.* **2017**, *404*, 188−196.

(21) Goryacheva, O. A.; Guhrenz, C.; Schneider, K.; Beloglazova, N. V.; Goryacheva, I. Y.; De Saeger, S.; Gaponik, N. Silanized luminescent quantum dots for simultaneous multicolour lateral flow immunoassay of two mycotoxins. *ACS Appl. Mater. Interfaces.* **2020**, *12*, 24575−24584.

(22) Panagiotopoulou, M.; Salinas, Y.; Beyazit, S.; Kunath, S.; Duma, L.; Prost, E.; Mayes, A. G.; Resmini, M.; Tse Sum Bui, B.; Haupt, K. Molecularly imprinted polymer coated quantum dots for multiplexed cell targeting and imaging. *Angew. Chem., Int. Ed.* **2016**, *55*, 1−6.

(23) Darbandi, M.; Urban, G.; Krüger, M. A facile synthesis method to silica coated CdSe/ZnS nanocomposites with tuneable size and optical properties. *J. Colloid Interface Sci.* **2010**, *351*, 30−34.

(24) Zhang, B.; Wang, X.; Liu, F.; Cheng, Y.; Shi, D. Effective reduction of nonspecific binding by surface engineering of quantum dots with bovine serum albumin for cell-targeted imaging. *Langmuir* **2012**, *28*, 16605−16613.

(25) Wen, C. Y.; Xie, H. Y.; Zhang, Z. L.; Wu, L. L.; Hu, J.; Tang, M.; Wu, M.; Pang, D. W. Fluorescent/magnetic micro/nano-spheres based on quantum dots and/or magnetic nanoparticles: preparation, properties, and their applications in cancer studies. *Nanoscale* **2016**, *8*, 12406−12429.

(26) Li, J.; Lv, Y.; Li, N.; Wu, R.; Xing, M.; Shen, H.; Li, L. S.; Chen, X. Robust synthesis of bright multiple quantum dot-embedded nanobeads and its application to quantitative immunoassay. *Chem. Eng. J.* **2019**, *361*, 499−507.

(27) Li, J.; Lv, Y.; Li, N.; Wu, R.; Li, J.; You, J.; Shen, H.; Chen, X.; Li, L. S. Dual protecting encapsulation synthesis of ultrastable quantum-dot nanobeads for sensitive and accurate detection of cardiac biomarkers. *Sensor Actuat B-Chem.* **2021**, *344*, 130275.

(28) Peters, A. L.; Davidson, M. B.; Schriger, D. L. A clinical approach for the diagnosis of diabe tes mellitus: an analysis using glycosylated hemoglobin levels. *Jama* **1996**, *276*, 1246−1252.

(29) Usta, D. D.; Salimi, K.; Pinar, A.; Coban, İ.; Tekinay, T.; Tuncel, A. A boronate affinity-assisted sers tag equipped with a sandwich system for detection of glycated hemoglobin in the hemolysate of human erythrocytes. *ACS Appl. Mater. Interfaces.* **2016**, *8*, 11934−11944.

(30) Zhang, H.; Li, D.; Yang, Y.; Chang, H.; Simone, G. On-resonance islands of Ag-nanowires sense the level of glycated hemoglobin for diabetes diagnosis. *Sensor Actuat B-Chem.* **2020**, *321*, 128451.

(31) Shen, H.; Wang, H.; Tang, Z.; Niu, J. Z.; Lou, S.; Du, Z.; Li, L. S. High quality synthesis of monodisperse zinc-blende CdSe and

CdSe/ZnS nanocrystals with a phosphine-free method. *CrystEngComm.* **2009**, *11*, 1733−1738.
(32) Riegler, J.; Nann, T. Application of luminescent nanocrystals as labels for biological molecules. *Anal. Bioanal. Chem.* **2004**, *379*, 913−919.
(33) Stöber, W.; Fink, A.; Bohn, E. Controlled growth of monodisperse silica spheres in the micron size range. *J. Colloid Interface Sci.* **1968**, *26*, 62−69.
(34) Chen, L.; Chen, C.; Li, R.; Li, Y.; Liu, S. CdTe quantum dot functionalized silica nanosphere labels for ultrasensitive detection of biomarker. *Chem. Commun.* **2009**, *19*, 2670−2672.
(35) Lv, Y.; Li, J.; Wu, R.; Wang, G.; Wu, M.; Shen, H.; Li, L. S. Silica-encapsulated quantum dots for highly efficient and stable fluorescence immunoassay of C-reactive protein. *Biochem. Eng. J.* **2018**, *137*, 344−351.
(36) Liu, H.; Crooks, R. M. Determination of percent hemoglobin A1c using a potentiometric method. *Anal. Chem.* **2013**, *85*, 1834−1839.
(37) Ahn, K. S.; Lee, J. H.; Park, J. M.; Choi, H. N.; Lee, W. Y. Luminol chemiluminescence biosensor for glycated hemoglobin (HbA1c) in human blood samples. *Biosens. Bioelectron.* **2016**, *75*, 82−87.
(38) Cerqueira, L. B.; Fachi, M. M.; Kawagushi, W. H.; Pontes, F. L. D.; de Campos, M. L.; Pontarolo, R. New validated method for quantification of glycated hemoglobin by LC-QToF-MS: is HRMS able to quantify clinical samples? *J. Am. Soc. Mass Spectrom.* **2020**, *31*, 1172−1179.
(39) Yan, S. T.; Xiao, H. Y.; Tian, H.; Li, C. L.; Fang, F. S.; Li, X. Y.; Cheng, X. L.; Li, N.; Miao, X. Y.; Yang, Y.; Wang, L. C.; Zou, X. M.; Ma, F. L.; He, Y.; Sai, X. Y. The cutoffs and performance of glycated hemoglobin for diagnosing diabetes and prediabetes in a young and middle-aged population and in an elderly population. *Diabetes Res. Clin. Pract.* **2015**, *109*, 238−245.
(40) Wang, S.; Niu, J.; Zhao, Z.; Xu, M.; Lu, J.; Li, M.; Wang, T.; Chen, Y.; Wang, S.; Dai, M.; Zheng, R.; Zhu, Y.; Wang, W.; Ning, G.; Bi, Y.; Xu, Y. Detection of diabetes and prediabetes using glycosylated hemoglobin in Chinese adults living in Shanghai: A prospective analysis. *J. Diabetes* **2020**, *12*, 573−582.

https://doi.org/10.1021/acs.langmuir.2c00392
Langmuir 2022, 38, 4969−4978